Tunable Lamb wave band gaps in two-dimensional magnetoelastic phononic crystal slabs by an applied external magnetostatic field

Changjiang Zhou, Yi Sai, Jiujiu Chen*

State Key Laboratory of Advanced Design and Manufacturing for Vehicle Body, College of Mechanics and Vehicle Engineering, Hunan University, Changsha City 410082, PR China

Abstract

This paper theoretically investigate the band gaps of Lamb mode waves in two-dimensional magnetoelastic phononic crystal slabs by an applied external magnetostatic field. With the assumption of uniformly oriented magnetization, an equivalent piezomagnetic material model is used. The effects of magnetostatic field on phononic crystals are considered carefully in this model. The numerical results indicate that the width of the first band gap is significantly changed by applying the external magnetic field with different amplitude, and the ratio between the maximum and minimum gap widths reaches 228%. Further calculations demonstrate that the orientation of the magnetic field obviously affect the width and location of the first band gap. The contactless tunability of the proposed phononic crystal slab shows many potential applications of vibration isolation in engineering.

Keywords: Tunability, Lamb wave band gap, magnetoelastic phononic crystal slabs, applied external magnetostatic field

1. Introduction

Phononic crystals (PCs) are functional periodic structures which consist of materials with different elastic properties. They have attracted considerable research since they exhibit multi-physical phenomena, such as the negative refraction [1-2], localized defect modes [3-4], complete frequency gaps [5-10]. Elastic waves of any modes within the complete frequency gaps are forbidden to propagate along any direction. This confers to PCs potential applications in acoustic wave reflectors, filters,

*Corresponding author. E-mail: chen99nju@gmail.com; Tel.: 86-731-88823993.

switches, etc. Moreover, for yielding desirable operation properties, it's very necessary to control a frequency band gap explicitly and conveniently.

Recently, there has been a growing interest in using PCs with magnetic materials to tune band gaps [11-20]. For example, Wang *et al.* have investigated the elastic wave propagation in the magneto-electro-elastic phononic crystals and considered the effects of the piezoelectricity and piezomagnetism on the band structures [12]. Matar *et al.* have presented an equivalent piezomagnetic material model for the magnetoelastic PCs with external magnetostatic field [13-15]. Their results demonstrate that the external magnetic field can be applied to control the band gaps. Ding *et al.* have studied the influence of external magnetic field and pre-stress on the characteristics of band gaps of PCs based on the nonlinear constitutive equations of magnetostrictive materials [16]. After that, a mechanical-magneto-thermal model has been proposed by Zhang *et al,* and they suggest that the demagnetization effect should not be ignored [17]. Bayat *et al.* have investigated the band structure properties of a soft magnetorheological phononic crystal (PC) [18]. Their studies indicate that large deformations and external magnetic field could transform the location and width of band gaps.

Taking the coupling among magnetic, electric, pre-stress, temperature, and elastic phenomena into account, the studies above are very remarkable in reporting meaningful changes in the band structures of PCs. However, without considering the magnetic and mechanical boundary conditions, all of them have analyzed only the bulk waves. As is known to all, Lamb waves [21-25] propagated in PC slabs are extremely useful for various sensors, noncontact and nondestructive evaluation in industry. Therefore, the theoretical researches about the magnetoelastic PC slabs with external magnetostatic field have become necessary.

In order to investigate the effects of the external magnetostatic field on the magnetoelastic PC slabs, an equivalent piezomagnetic material model based on existing research is used. And the demagnetization effect is studied in detail. The first band gap (FBG) of Lamb mode waves in the homogenous brass slab with an array of square stubbed rods is considered just to simplify the physical model. With different

orientations and amplitude of the magnetostatic field, the tunability of the characteristics of the two-dimensional PC slabs is investigated in detail by using the finite element method (FEM). Through our researches, a kind of PC slabs, which can achieve contactless tuning of the complete band gap by using applied magnetic field, is obtained.

2. Theory

2.1. Model of the unit

The system considered in the computations is a square lattice of magnetoelastic square stubbed rod deposited on a homogenous slab, as depicted in Fig. 1. The constant of lattice of the phononic crystal is a and the length of the side of the square stubbed rod is d. The z-axis is chosen to be perpendicular to the slab and parallel to the rod length. The length of the square stubbed rod is denoted by h_1 and the thickness of the slab is denoted by h_2.

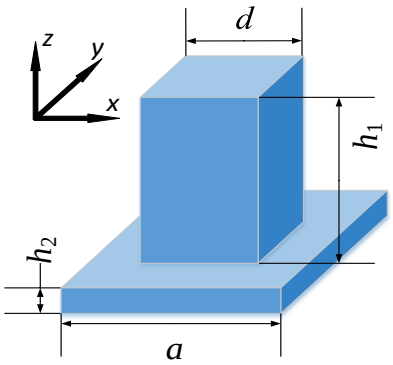

Fig. 1. Schematic diagram of the square unit cell of a homogeneous slab with the magnetoelastic square stubbed rods.

A magneto-elastic wave in a cubic ferromagnet magnetized to saturation is considered here. In the inhomogeneous linear elastic medium without body force, its propagation can be described by the piezomagnetic constitutive equations as [14, 20]:

$$\rho \frac{\partial^2 u_i}{\partial t^2} = \frac{\partial \sigma_{ij}}{\partial x_j}, \tag{1}$$

$$\frac{\partial b_i}{\partial x_i} = 0 \ , \tag{2}$$

$$\sigma_{ij} = c_{ijkl} \frac{\partial u_k}{\partial x_l} + q_{lij} \frac{\partial \varphi_m}{\partial x_l}, \tag{3}$$

$$b_i = q_{ikl} \frac{\partial u_k}{\partial x_l} - \mu_{il} \frac{\partial \varphi_m}{\partial x_l}. \tag{4}$$

where $i, j, k, l = x, y, z$. ρ, u_i, b_i, x_i, σ_{ij}, c_{ilkl}, q_{lij}, φ_m and μ_{il} are the mass density, particle displacement, magnetic induction, Eulerian coordinates, stress tensor components, elastic constants, piezomagnetic tensor, magnetic potential, and magnetic permeability matrix, respectively. The surface and interface boundary conditions have to be specified to calculate the dispersion relations with the unit cell. The interfacial condition between two materials is considered to be perfect. That is to say, the potential of the magnetic field and the displacement in two phases are continuous at the interface. The top surface and all sides of the square stubbed rod are set to be stress free which requires nullity of mechanical stress. To consider the demagnetization effect and the vacuum environment in which the PC slabs are studied, the open-circuit magnetic boundary conditions [20] is enforced on the surface regions of the magnetoelastic inclusion.

2.2. The influence of the applied external magnetostatic field

First, we consider the case where an external magnetostatic field is applied along one of the crystallographic axis of the PC slabs (Fig. 2). To be able to consider the varying amplitude of the applied magnetic field, we use an equivalent piezomagnetic material model with field dependent effective elastic constants C_{ijkl}^{H}, piezomagnetic constants q_{lij} and magnetic permeability μ_{ij}. With the assumption of uniformly oriented magnetization, the model is studied at the square rods of infinite length. When the magnetic field H_z is applied along *z*-axis, the only changed elastic elastic constants, piezomagnetic constants, and magnetic permeabilities are given by [15]:

$$C_{44}^{H}=C_{55}^{H}=C_{44}-\frac{B_2^2}{4\mu_0 M_s(H_0+\frac{2K_1}{\mu_0 M_s}+\frac{2B_1^2}{\mu_0 M_s\left(C_{11}-C_{12}\right)})}, \tag{5}$$

$$q_{24}=q_{15}=-\frac{B_2}{2(H_0+\frac{2K_1}{\mu_0 M_s}+\frac{2B_1^2}{\mu_0 M_s\left(C_{11}-C_{12}\right)})}, \tag{6}$$

$$\mu_{11}=\mu_{22}=\mu_0(1+\frac{M_s}{H_0+\frac{2K_1}{\mu_0 M_s}+\frac{2B_1^2}{\mu_0 M_s\left(C_{11}-C_{12}\right)}}),\quad \mu_{33}=\mu_0. \tag{7}$$

where μ_0, M_s, K_1, $B_1\left(B_2\right)$ and H_0 are the magnetic permeability of vacuum, the saturation magnetization, the magnetic anisotropy constants, the magneto-elastic constants and the internal magnetic field, respectively.

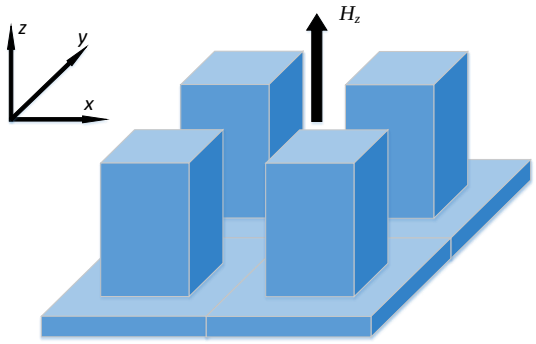

Fig. 2. Schematic view of the PC slabs with the applied external magnetic field along the *z*-axis

In Eqs. (5)–(7), the internal magnetic field H_0 is the sum of the external magnetic field H_z and the demagnetizing field H_D. According to the assumption and the consideration of the model, the demagnetizing field H_D is the only term related to the geometrical shape and size of the rods. Therefore, the use of the model is valid when the demagnetizing field is handled correctly in our studies.

When the applied magnetic field is along the *z*-axis, the influence of the demagnetizing field of the neighboring stubbed rods is negligible. Therefore, an isolated rod is considered here, and its demagnetizing field H_D is given by [26]:

$$H_D=-N\cdot M. \tag{8}$$

where N is the demagnetizing factor, and M is the magnetization intensity. In the case of a square stubbed rod of finite length h_1, oriented along the *z*-axis, the simple and approximate demagnetizing factor is [27]:

$$N_z = \frac{1}{2n+1}. \tag{9}$$

where $n = h_1 / d$ is the dimensional ratio. This expression remains a good approximation as soon as $0.5 \le n \le 2$.

Then, we consider the case where an external magnetostatic field H_x is applied along the *x*-axis of the PC slabs. The only changed parameters of the equivalent piezomagnetic material have the same expressions with Eqs. (5)–(7), just applying an index permutation. Moreover, when the magnetic field is applied perpendicularly to the rod axis, *i.e.*, the *x*-axis of the PC, the demagnetizing field is more complicated than the former case, and the neighboring square stubbed rods have significant influence.

In order to investigate the influence of the magnetostatic field of the surrounding magnetoelastic rods on the demagnetizing field, we consider the internal magnetostatic field in the square stubbed rods, which are placed in a periodic rectangular lattice, as shown in Fig. 2. With the magnetization along the *x*-axis, in fact, the *x* component of the internal magnetostatic field H_x^{in} has been derived by Tsymbal. And it is given by [28]:

$$\begin{aligned} H_x^{in}(x,y,z) = \frac{M_s}{a^2}\Bigg\{ & \sum_{m=1}^{\infty} \frac{d}{k_2}\left[\sin k_2(y-d) - \sin k_2 y\right] \\ & \times\left[2 - e^{-k_2 z} - e^{k_2(z-h_1)}\right] - \sum_{n,m=1}^{\infty} \frac{2k_2}{k^2 k_1}\left[\sin k_1(x-d) - \sin k_1 x\right] \\ & \times\left[\sin k_2(y-d) - \sin k_2 y\right]\times\left[2 - e^{-kz} - e^{k(z-h_1)}\right]\Bigg\}. \end{aligned} \tag{10}$$

where $k_1 = 2\pi n / a$, $k_2 = 2\pi m / a$ and $k = \sqrt{k_1^2 + k_2^2}$. Here, we shall be interested in the demagnetizing field which is the average of the internal magnetostatic field over the volume of the square stubbed rod. And it is determined by:

$$H_D = \left\langle H_x^{in} \right\rangle = \frac{1}{d^2 h_1} \int_0^{\mathrm{d}} \int_0^{d} \int_0^{h_1} H_x^{in}(x, y, z)\, dz dy dx, \tag{11}$$

Computing this integral we obtain:

$$\begin{aligned} H_D = -\frac{8M_s}{a^2 d^2} \Bigg\{ & \sum_{m=1}^{\infty} \frac{d^2}{k_2^2} \sin^2\left(\frac{k_2 d}{2}\right) \left[1 - \frac{1 - e^{-k_2 h_1}}{k_2 h_1}\right] \\ & + 8 \sum_{n,m=1}^{\infty} \frac{1}{k^2 k_1^2} \sin^2\left(\frac{k_1 d}{2}\right) \sin^2\left(\frac{k_2 d}{2}\right) \left[1 - \frac{1 - e^{-k h_1}}{k h_1}\right] \Bigg\}. \end{aligned} \tag{12}$$

The summation of this series in Eq. (12) is made by computer. And figure 3 shows the calculated demagnetizing field for the array of the square stubbed rods as a function of the ratio h_1 / d. As is evident from this figure, the demagnetizing field sharply decreases at first and finally reaches a plateau with the ratio increasing. In the limit of large ratio the magnetoelastic rods can be considered as the rods in infinite length. Compared with the result (-0.21875) of the infinitely long square rods [29], the validity of Eq. (12) has been justified.

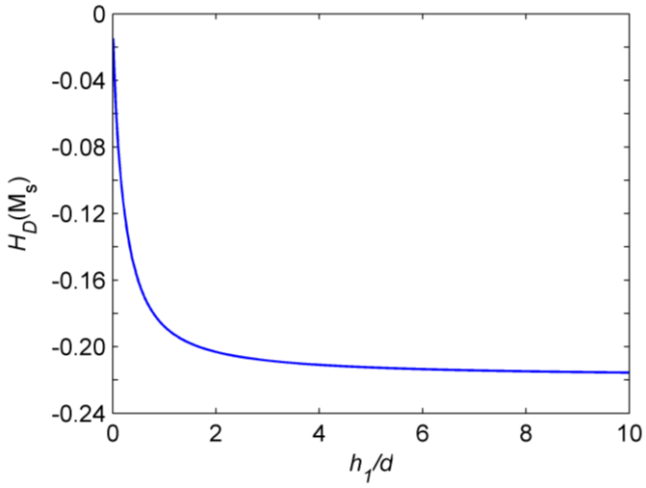

Fig. 3. The calculated demagnetizing field for the array of the magnetoelastic square stubbed rods as a function of the ratio h_1 / d

3. Numerical Results and Discussion

3.1. The effective parameters of the equivalent piezomagnetic material

Figure 4 shows the curves of the only changed effective elastic constants, piezomagnetic constants, and magnetic permeabilities for a Terfenol-D rod of the

periodic array as a function of the amplitude of an external magnetic field (applied along the *z*-axis and along the *x*-axis), with $a = 2\,\text{mm}$, $h_1 = 1.5\,\text{mm}$, $h_2 = 0.2\,\text{mm}$ and $d = 1.5mm$. The material parameters of Terfenol-D are chosen as following: $\rho_0 = 9210\ \text{kg/m}^3$, $C_{11} = 82\ \text{GPa}$, $C_{12} = 40\ \text{GPa}$, $C_{44} = 48\ \text{GPa}$, $M_s = 8\times10^5\ \text{A/m}$, $K_1 = 4\times10^5\ \text{J/m}^3$, $B_1 = -2\times10^7\ \text{J/m}^3$, and $B_2 = -3.456\times10^8\ \text{J/m}^3$ [15]. In addition, the Eqs. (5)–(7) based on the equivalent piezomagnetic material model become doubtful when the amplitude of the external magnetic field close to the condition of avoiding the magnetic spin reorientation transition. Therefore, the amplitude is limited in the range of $4 \le H_z\,(H_x) \le 20\,\text{kOe}$ in this paper.

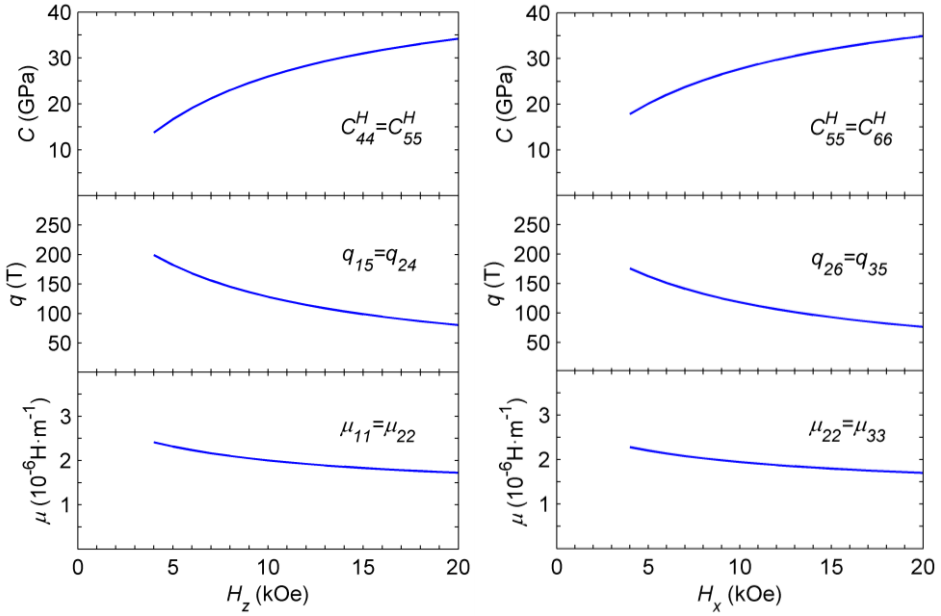

(a) (b)

Fig. 4. The only changed elastic constants, piezomagnetic constants, and magnetic permeabilities for a Terfenol-D rod of the periodic array as a function of the amplitude of an external magnetic field (a) along the *z*-axis and (b) along the *x*-axis of the unit cell.

3.2. Band structures and transmission spectra

Firstly, we show the band structures of the system in the previous examples with an external magnetic field $H_z = 5\,\text{kOe}$ along the *z*-axis. Figure 5 displays the band

structures (the plot is given as the frequency (KHz) to reduced wave vector $k\pi/a$ calculated by FEM) along the high symmetry axes of the first BZ, i.e., along the ΓXMΓ path. According to the Bloch theorem, this is sufficient to determine the complete frequency band gaps. The homogenous slab is assumed to be made of brass, with the following parameters: ρ_0=8600 kg/m^3, $C_{11}=166.50$ GPa, $C_{12}=90.64$ GPa, $C_{44}=37.93$ GPa [30]. It exists a complete elastic band gap in the 0–700KHz frequency range, as shown in Fig. 5(a), within which the vibration and propagation of waves of any polarization and incidence are not allowed. The FBG extends from 371.7 to 495.6 KHz. The gap width (corresponding relative bandwidth) is 123.9 KHz (28.57%).

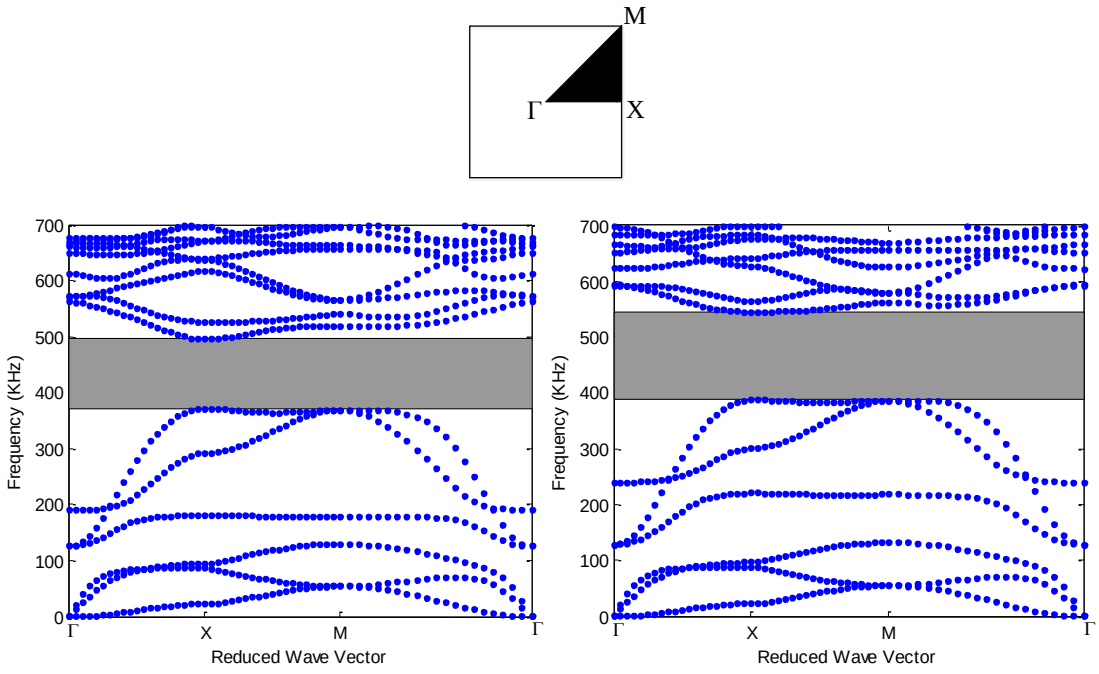

(a) (b)

Fig. 5. Dispersion relations of a homogenous brass slab with the Terfenol -D rods applied different magnetic fields along the *z*-axis. (a) $H_z=5$ kOe, (b) H_z=15 kOe.

Secondly, in order to verify the correctness of the band structures, the transmission spectra are used in the following example. Figure 6(a) shows the same band structures of Fig. 5(a) along the ΓX direction in the 0–700KHz frequency range. At the same time, the corresponding transmission spectra are given in Fig. 6(b).

The location and width of the band gaps exhibits very good agreement between the band structures and the transmission spectra.

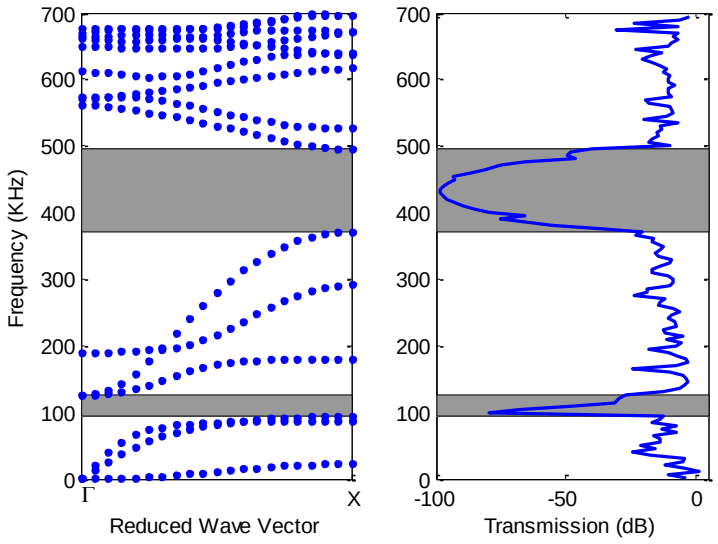

(a) (b)

Fig. 6. The same band structures (a) of Fig. 5(a) and transmission power spectra (b) of Lamb wave modes along the ΓX direction.

Thirdly, to evaluate the effects of the amplitude of external magnetic field, other parameters will remain the same except H_z=15 kOe. Figure 5(b) shows that there is a complete band gap from 387.9 to 545.7 KHz in the 0–700KHz frequency range. The FBG width (corresponding relative bandwidth) is 157.8 KHz (33.80%). The magnetoelastic PC slabs with H_z=15 kOe enlarge the band width (relative bandwidth) of the FBG by a factor of 1.27 (1.18). There are several points should be noted. At first, the band gap is pushed to higher frequency region by changing the external magnetic field from 5 to 15 kOe. Furthermore, the band gap is significantly enlarged. At last, the dispersion curve of the lower edge of the band gap is flat.

Finally, the PC slabs with an external magnetic field along *x*-axis are considered. The anisotropy of the equivalent piezomagnetic material is enhanced by turning the magnetic field from the *z*-axis to the *x*-axis, and the changed irreducible BZ is shown in Fig. 7. The band structures along the ΓXMYΓ path exist a complete elastic band gap in the 0–700KHz frequency range, as shown in Fig. 7(a). To compare with the case of the external magnetic field along the *z*-axis, the dispersion curves displays

obvious anisotropy, and it has significant effects on the width of the FBG.

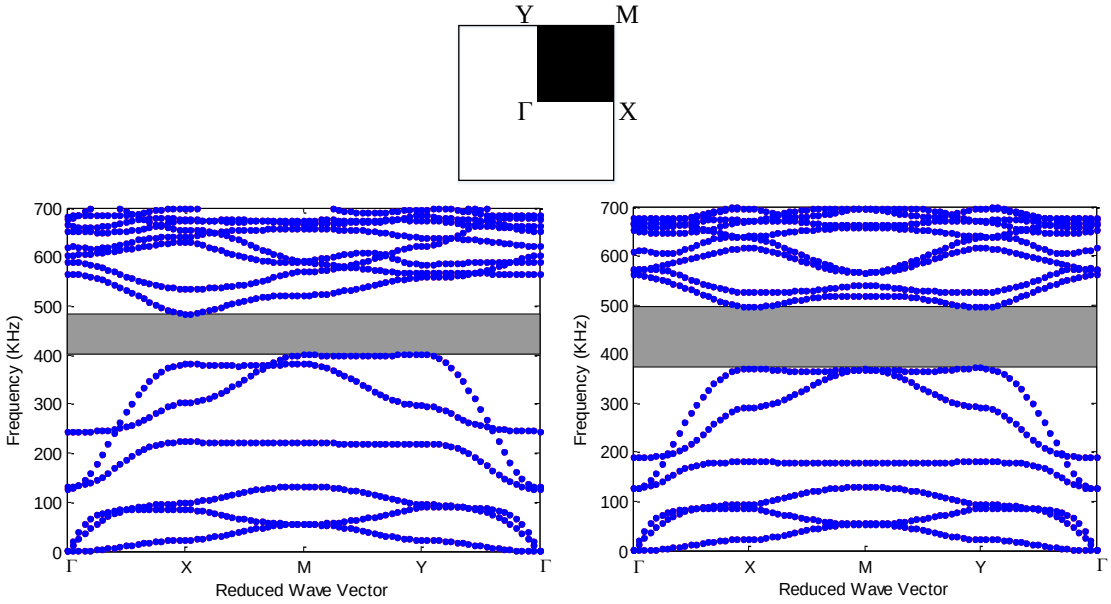

(a) (b)

Fig. 7. Dispersion relations of a homogenous brass slab with the Terfenol -D rods applied different magnetic fields (a) $H_x = 5\,\mathrm{kOe}$ along the *x*-axis, (b) $H_z = 5\,\mathrm{kOe}$ along the *z*-axis of the unit cell.

3.3. Band gap maps and discussion

As mentioned above, the numerical results demonstrate that the external magnetostatic field has significant effects on the FBG. The further investigation about the effects of the amplitude and the orientation of the magnetic field on the FBG is necessary.

The FBG maps of the PC slabs in the amplitude range $4 \le H_z\,(H_x) \le 20\,\mathrm{kOe}$ are displayed in Fig. 8. In both of the two cases in different orientations of the external magnetic field, the changing trends of the FBG are the same. And, just like the variation of the effective elastic constants with the magnetic field increasing in Fig. 4, the FBG widths of them first increase gradually and finally reach a plateau. It is worth noting that the mid-gaps of the two cases are pushed to higher frequency region due to the value of the equivalent stiffness increasing with the magnetic field increasing. And the variation of stiffness can change the resonance frequencies of the PC slabs. In other words, because the band structure originates from the interaction between the

Braggscattering waves and the radiation waves from vibrating PC slabs, the FBG of the proposed magnetoelastic PC slabs can be tuned by applying external magnetic field with different amplitude. Additionally, we should note that the lower edge of band gaps, especially in the case along the *x*-axis, is almost unchanged.

By comparing the two cases as shown in Fig. 8, it is obvious that the variation of the width and edges of the FBG in the case along the *x*-axis is stronger than the other case. This is mainly because that the anisotropy of the equivalent piezomagnetic material becomes stronger by turning the magnetic field from the *z*-axis to the *x*-axis. As shown in Fig. 8(a), the gap width increases sharply in the amplitude range 4–9 kOe, corresponding to an average variation ratio of 10.35 KHz/kOe. At the range of 10–20 kOe, the variation ratio reduces to below 1 KHz/kOe. The proposed PC slabs show a good tunability at low magnetic field. When the magnetostatic field turn to the *x*-axis, the range of sharply increase is enlarged to 4–14 kOe, and the ratio between the maximum and minimum value of the gap widths reach 228%. This approach of tuning band structures is useful to control wave propagation for smart structure applications.

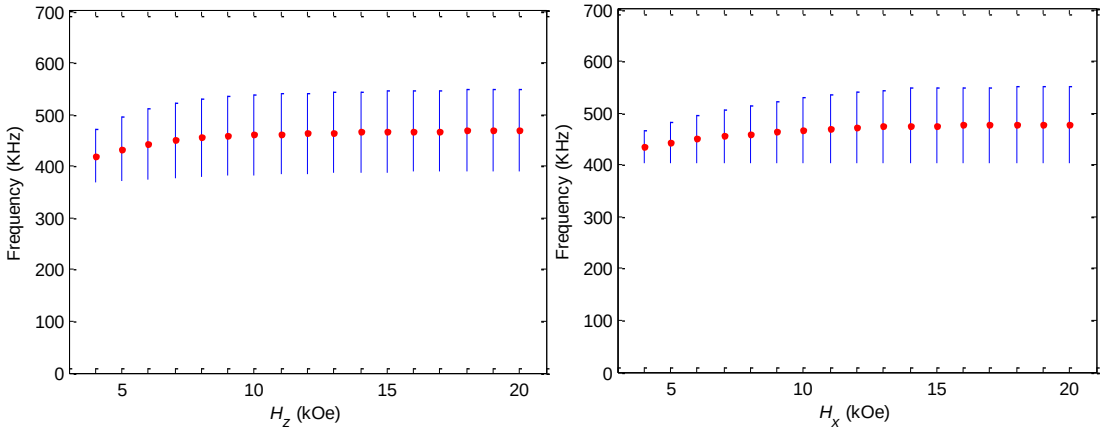

(a) (b)

Fig. 8. The dependence of the band gap maps of the PC slabs on the amplitude of the applied external magnetostatic field (a) along the *z*-axis and (b) along the *x*-axis of the unit cell.

4. Conclusion

In summary, based on an equivalent piezomagnetic material model, the band structure properties of a square lattice of magnetoelastic square stubbed rods

deposited on a homogenous slab are obtained by varying the amplitude and the orientation of the external magnetostatic field. For the ferromagnet magnetized to saturation, demagnetization effect cannot be ignored. The numerical results indicate that the magnetic field has a significant influence on the effective parameters of the Terfenol-D square stubbed rods. The width of the FBG increases at first and finally reaches a plateau with the magnetic field increasing. As comparison, changing the orientation of the magnetic field from the *z*-axis to the *x*-axis, the band gaps of the system are investigated. The results reveal that the variation of the gap width becomes stronger than the former case. And the PC slabs behave as a switch controlled by changing the direction and amplitude of the magnetic field. This proposed model shows the good flexibility in practical design and optimization of such PC-based devices, and opens the possibility of easy controllability of the properties of PC slabs without any contact.

Acknowledgements

The authors gratefully acknowledge financial support from National Science Foundation of China under Grant No.11374093 and 51275160, the Program of the State Key Laboratory of Advanced Design and Manufacturing for Vehicle Body No.71375006, and the Hunan University Young Teacher Growth Scheme Funding.

References

[1] X.D. Zhang and Z.Y. Liu, Negative refraction of acoustic waves in two-dimensional phononic crystals, Appl. Phys. Lett. 85 (2004) 341-343.

[2] A.-C. Hladky-Hennion, J.O. Vasseur, G. Haw, C. Croënne, L. Haumesser, and A.N. Norris, Negative refraction of acoustic waves using a foam-like metallic structure, Appl. Phys. Lett. 102 (2013) 144103~1-4.

[3] Z. Lazcano, O. Meza and J. Arriaga, Localization of acoustic modes in periodic porous silicon structures, Nanoscale Res. Lett. 9 (2014) 419~1-9.

[4] Y. He, F.G. Wu, Y.W. Yao, X. Zhang, Z.F. Mu, S.Y Yan, C. Cheng, Effect of defect configuration on the localization of phonons in two-dimensional phononic crystals, Phys. Lett. A 377 (2013) 889-894.

[5] Z.Y. Liu, X.X. Zhang, Y.W. Mao, Y.Y. Zhu, Z.Y. Yang, C.T. Chan, P. Sheng, Locally resonant sonic materials, Science 289 (2000) 1734-1736.

[6] Z.G. Huang, Z.Y. Chen, Acoustic waves in two-dimensional phononic crystals with reticular geometric structures, J. Vib. Acoust. 133 (2011) 031011~1-6.

[7] J.J. Chen, Y.J. Xia, X. Han, H.B. Zhang, Lamb waves in phononic crystal slabs: truncated plane parallels to the axis of periodicity, Ultrasonics 52 (2012) 920-924.

[8] H.B. Zhang, J.J. Chen, X. Han, Lamb wave band gaps in a homogenous plate with periodic tapered surface, J. Appl. Phys. 112 (2012) 054503~1-6.

[9] J.J. Chen, H.B. Zhang, and X. Han, Local resonance broadband gap in a homogeneous plate with periodic truncated cones, Jpn. J. Appl. Phys. 52 (2013) 034301~1-4.

[10] Z.G. Huang, Silicon-based filters, resonators and acoustic channels with phononic crystal structures, J. Phys. D: Appl. Phys. 44 (2011) 245406~1-9.

[11] X. Guo, P.J. Wei, Dispersion relations of elastic waves in one-dimensional piezoelectric/piezomagnetic phononic crystal with initial stresses, Ultrasonics 66 (2016) 72-85.

[12] Y. Z. Wang, F.M. Li, W.H. Huang, X.A. Jiang, Y.S. Wang, K. Kishimoto, Wave band gaps in two-dimensional piezoelectric/piezomagnetic phononic crystals, Int. J. Solids Struct. 45 (2008) 4203-4210.

[13] J.F. Robillard, O. Bou Matar, J.O. Vasseur, P.A. Deymier, M. Stippinger, A.-C. Hladky-Hennion, Y. Pennec, and B. Djafari-Rouhani, Tunable magnetoelastic phononic crystals, Appl. Phys. Lett. 95 (2009) 124104~1-3.

[14] J. O. Vasseur, O. Bou Matar, J.F. Robillard, A.-C. Hladky-Hennion, P.A. Deymier, Band structures tunability of bulk 2D phononic crystals made of magneto-elastic materials, AIP Adv. 1 (2011) 041904~1-12.

[15] O. Bou Matar, J.F. Robillard, J.O. Vasseur, A.-C. Hladky-Hennion, P.A. Deymier, P. Pernod, and V. Preobrazhensky, Band gap tunability of magneto-elastic phononic crystal, J. Appl. Phys. 111 (2012) 054901~1-14.

[16] R. Ding, X.L. Su, J.J. Zhang, and Y.W. Gao, Tunability of longitudinal wave band gaps in one dimensional phononic crystal with magnetostrictive material, J. Appl.

Phys. 115 (2014) 074104~1-8.

[17] S.Z. Zhang, Y. Shi, and Y.W. Gao, A mechanical-magneto-thermal model for the tunability of band gaps of epoxy/TerfenolD phononic crystals, J. Appl. Phys. 118 (2015) 034101~1-8.

[18] A. Bayat and F. Gordaninejad, Band-gap of a soft magnetorheological phononic crystal, J. Vib. Acoust. 137 (2015) 011011~1-8.

[19] A.C. Yang, P. Li, Y.M. Wen, C. Yang, D.C. Wang, F. Zhang, and J.J. Zhang, Low-magnetic-threshold acoustic switch fabricated utilizing magnetoelastic FeNi/brass phononic crystal plate, Appl. Phys. Express 8 (2015) 097201~1-3.

[20] X.H. Wu, Y.P. Shen, Q. Sun, Lamb wave propagation in magnetoelectroelastic plates, Appl. Acoust. 68 (2007) 1224-1240.

[21] T.T. Wu, Z.G. Huang, T.C. Tsai, and T.C. Wu, Evidence of complete band gap and resonances in a plate with periodic stubbed surface, Appl. Phys. Lett. 93 (2008) 111902~1-3.

[22] J.C. Hsu, T.T. Wu, Efficient formulation for bandstructure calculations of two-dimensional phononic-crystal plates, Phys. Rev. B 74 (2006) 144303~1-8.

[23] A. Khelif, B. Aoubiza, S. Mohammadi, A. Adibi, and V. Laude, Complete band gaps in two-dimensional phononic crystal slabs, Phys. Rev. E 74 (2006) 046610~1-5.

[24] J. O. Vasseur, A.-C. Hladky-Hennion, B. Djafari-Rouhani, F. Duval, B. Dubus, Y. Pennec, and P. A. Deymier, Waveguiding in two-dimensional piezoelectric phononic crystal plates, J. Appl. Phys. 101 (2007) 114904~1-6.

[25] Y.F. Zhu, Y. Yuan, X.Y. Zou, J.C. Cheng, Piezoelectric-sensitive mode of lamb wave in one-dimensional piezoelectric phononic crystal plate, Wave Motion 54 (2015) 66-75.

[26] R.C. O'handley, Modern Magnetic Materials Principle and Applications, John Wiley & Sons, Inc., New York, 2000.

[27] M. Sato and Y. Ishii, Simple and approximate expressions of demagnetizing factors of uniformly magnetized rectangular rod and cylinder, J. Appl. Phys. 66 (1989) 983-985.

[28] E.Y. Tsymbal, Theory of magnetostatic coupling in thin-film rectangular magnetic elements, Appl. Phys. Lett. 77 (2000) 2740-2742.

[29] V.A. Ignatchenko, H. Kronmüller, and M. Grönefeld, Magnetostatic coupling of two-dimensional periodic arrangements of single domain particles, J. Magn. Magn. Mater. 89 (1990) 229-235.

[30] R. Hao, C.Y. Qiu, Y.T. Ye, C.H. Li, H. Jia, M.Z. Ke, and Z.Y. Liu, Transmission enhancement of acoustic waves through a thin hard plate embedded with elastic inclusions, Appl. Phys. Lett. 101 (2012) 021910~1-4.